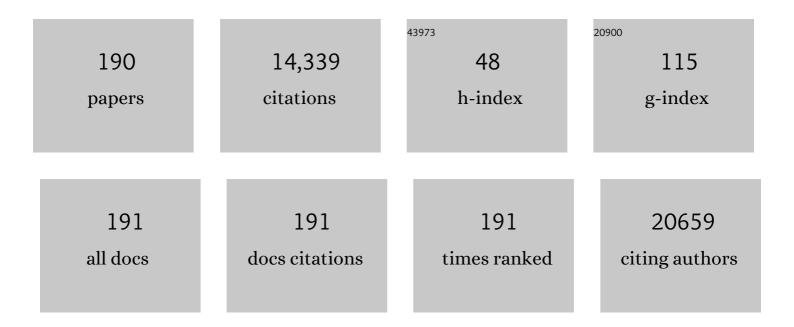
Seung Hong Choi

List of Publications by Year in descending order

Source: https://exaly.com/author-pdf/2591932/publications.pdf Version: 2024-02-01



SELING HONG CHOL

#	Article	IF	CITATIONS
1	A graphene-based electrochemical device with thermoresponsive microneedles for diabetes monitoring and therapy. Nature Nanotechnology, 2016, 11, 566-572.	15.6	1,394
2	Stretchable silicon nanoribbon electronics for skin prosthesis. Nature Communications, 2014, 5, 5747.	5.8	1,145
3	Wearable/disposable sweat-based glucose monitoring device with multistage transdermal drug delivery module. Science Advances, 2017, 3, e1601314.	4.7	836
4	Large-Scale Synthesis of Uniform and Extremely Small-Sized Iron Oxide Nanoparticles for High-Resolution <i>T</i> ₁ Magnetic Resonance Imaging Contrast Agents. Journal of the American Chemical Society, 2011, 133, 12624-12631.	6.6	835
5	Uniform Mesoporous Dye-Doped Silica Nanoparticles Decorated with Multiple Magnetite Nanocrystals for Simultaneous Enhanced Magnetic Resonance Imaging, Fluorescence Imaging, and Drug Delivery. Journal of the American Chemical Society, 2010, 132, 552-557.	6.6	687
6	Continuous O ₂ -Evolving MnFe ₂ O ₄ Nanoparticle-Anchored Mesoporous Silica Nanoparticles for Efficient Photodynamic Therapy in Hypoxic Cancer. Journal of the American Chemical Society, 2017, 139, 10992-10995.	6.6	616
7	Nonblinking and Nonbleaching Upconverting Nanoparticles as an Optical Imaging Nanoprobe and T1 Magnetic Resonance Imaging Contrast Agent. Advanced Materials, 2009, 21, 4467-4471.	11.1	548
8	Nanoâ€6ized CT Contrast Agents. Advanced Materials, 2013, 25, 2641-2660.	11.1	522
9	Theranostic Probe Based on Lanthanideâ€Doped Nanoparticles for Simultaneous In Vivo Dualâ€Modal Imaging and Photodynamic Therapy. Advanced Materials, 2012, 24, 5755-5761.	11.1	367
10	Large-Scale Synthesis of Bioinert Tantalum Oxide Nanoparticles for X-ray Computed Tomography Imaging and Bimodal Image-Guided Sentinel Lymph Node Mapping. Journal of the American Chemical Society, 2011, 133, 5508-5515.	6.6	316
11	Gliomas: Histogram Analysis of Apparent Diffusion Coefficient Maps with Standard- or High- <i>b</i> -Value Diffusion-weighted MR Imaging—Correlation with Tumor Grade. Radiology, 2011, 261, 882-890.	3.6	297
12	Water-Dispersible Ferrimagnetic Iron Oxide Nanocubes with Extremely High <i>r</i> ₂ Relaxivity for Highly Sensitive in Vivo MRI of Tumors. Nano Letters, 2012, 12, 3127-3131.	4.5	269
13	Multifunctional Fe ₃ O ₄ /TaO _{<i>x</i>} Core/Shell Nanoparticles for Simultaneous Magnetic Resonance Imaging and X-ray Computed Tomography. Journal of the American Chemical Society, 2012, 134, 10309-10312.	6.6	219
14	Bioresorbable Electronic Stent Integrated with Therapeutic Nanoparticles for Endovascular Diseases. ACS Nano, 2015, 9, 5937-5946.	7.3	203
15	Magnetosome-like ferrimagnetic iron oxide nanocubes for highly sensitive MRI of single cells and transplanted pancreatic islets. Proceedings of the National Academy of Sciences of the United States of America, 2011, 108, 2662-2667.	3.3	183
16	Electromechanical cardioplasty using a wrapped elasto-conductive epicardial mesh. Science Translational Medicine, 2016, 8, 344ra86.	5.8	181
17	An endoscope with integrated transparent bioelectronics and theranostic nanoparticles for colon cancer treatment. Nature Communications, 2015, 6, 10059.	5.8	159
18	Glioma: Application of Whole-Tumor Texture Analysis of Diffusion-Weighted Imaging for the Evaluation of Tumor Heterogeneity. PLoS ONE, 2014, 9, e108335.	1.1	159

#	Article	IF	CITATIONS
19	Incorporating diffusion- and perfusion-weighted MRI into a radiomics model improves diagnostic performance for pseudoprogression in glioblastoma patients. Neuro-Oncology, 2019, 21, 404-414.	0.6	153
20	Iron oxide nanoclusters for T 1 magnetic resonance imaging of non-human primates. Nature Biomedical Engineering, 2017, 1, 637-643.	11.6	151
21	Flexible, sticky, and biodegradable wireless device for drug delivery to brain tumors. Nature Communications, 2019, 10, 5205.	5.8	148
22	Differentiation of True Progression from Pseudoprogression in Glioblastoma Treated with Radiation Therapy and Concomitant Temozolomide: Comparison Study of Standard and High- <i>b</i> Value Diffusion-weighted Imaging. Radiology, 2013, 269, 831-840.	3.6	147
23	Tissue-like skin-device interface for wearable bioelectronics by using ultrasoft, mass-permeable, and low-impedance hydrogels. Science Advances, 2021, 7, .	4.7	144
24	Stretchable and Transparent Biointerface Using Cellâ€5heet–Graphene Hybrid for Electrophysiology and Therapy of Skeletal Muscle. Advanced Functional Materials, 2016, 26, 3207-3217.	7.8	123
25	Enhanced Chemodynamic Therapy by Cu–Fe Peroxide Nanoparticles: Tumor Microenvironment-Mediated Synergistic Fenton Reaction. ACS Nano, 2022, 16, 2535-2545.	7.3	120
26	Multipleâ€Interaction Ligands Inspired by Mussel Adhesive Protein: Synthesis of Highly Stable and Biocompatible Nanoparticles. Angewandte Chemie - International Edition, 2011, 50, 11360-11365.	7.2	117
27	Tumor-associated macrophages in cancer: recent advancements in cancer nanoimmunotherapies. Journal of Experimental and Clinical Cancer Research, 2022, 41, 68.	3.5	115
28	Differentiating Malignant from Benign Common Bile Duct Stricture with Multiphasic Helical CT. Radiology, 2005, 236, 178-183.	3.6	107
29	Soft implantable drug delivery device integrated wirelessly with wearable devices to treat fatal seizures. Science Advances, 2021, 7, .	4.7	107
30	Glioblastoma Treated with Concurrent Radiation Therapy and Temozolomide Chemotherapy: Differentiation of True Progression from Pseudoprogression with Quantitative Dynamic Contrast-enhanced MR Imaging. Radiology, 2015, 274, 830-840.	3.6	102
31	Diffusion-weighted MR Imaging for the Differentiation of True Progression from Pseudoprogression Following Concomitant Radiotherapy with Temozolomide in Patients with Newly Diagnosed High-grade Gliomas. Academic Radiology, 2012, 19, 1353-1361.	1.3	96
32	Large-Scale Synthesis of Ultrathin Manganese Oxide Nanoplates and Their Applications to T1 MRI Contrast Agents. Chemistry of Materials, 2011, 23, 3318-3324.	3.2	92
33	Evaluation of the microenvironmental heterogeneity in high-grade gliomas with IDH1/2 gene mutation using histogram analysis of diffusion-weighted imaging and dynamic-susceptibility contrast perfusion imaging. Journal of Neuro-Oncology, 2015, 121, 141-150.	1.4	92
34	Preoperative Magnetic Resonance Imaging Staging of Uterine Cervical Carcinoma. Journal of Computer Assisted Tomography, 2004, 28, 620-627.	0.5	86
35	Hepatocellular Carcinoma in Liver Transplantation Candidates: Detection with Gadobenate Dimeglumine–Enhanced MRI. American Journal of Roentgenology, 2008, 191, 529-536.	1.0	82
36	Prediction of IDH genotype in gliomas with dynamic susceptibility contrast perfusion MR imaging using an explainable recurrent neural network. Neuro-Oncology, 2019, 21, 1197-1209.	0.6	80

#	Article	IF	CITATIONS
37	True Progression versus Pseudoprogression in the Treatment of Glioblastomas: A Comparison Study of Normalized Cerebral Blood Volume and Apparent Diffusion Coefficient by Histogram Analysis. Korean Journal of Radiology, 2013, 14, 662.	1.5	79
38	Multifunctional mesoporous silica nanocomposite nanoparticles for pH controlled drug release and dual modal imaging. Journal of Materials Chemistry, 2011, 21, 16869.	6.7	78
39	Multifunctional Cell-Culture Platform for Aligned Cell Sheet Monitoring, Transfer Printing, and Therapy. ACS Nano, 2015, 9, 2677-2688.	7.3	72
40	Synthesis of Uniformly Sized Manganese Oxide Nanocrystals with Various Sizes and Shapes and Characterization of Their <i>T</i> ₁ Magnetic Resonance Relaxivity. European Journal of Inorganic Chemistry, 2012, 2012, 2148-2155.	1.0	71
41	A practical scoring system to determine whether to proceed with surgical resection in recurrent glioblastoma. Neuro-Oncology, 2013, 15, 1096-1101.	0.6	67
42	<i>In vivo</i> Imaging of Tumor Transduced with Bimodal Lentiviral Vector Encoding Human Ferritin and Green Fluorescent Protein on a 1.5T Clinical Magnetic Resonance Scanner. Cancer Research, 2010, 70, 7315-7324.	0.4	60
43	Histogram Analysis of Apparent Diffusion Coefficient Map of Standard and High B-value Diffusion MR Imaging in Head and Neck Squamous Cell Carcinoma. Academic Radiology, 2012, 19, 1233-1240.	1.3	59
44	Advances in drug delivery technology for the treatment of glioblastoma multiforme. Journal of Controlled Release, 2020, 328, 350-367.	4.8	58
45	The Role of Perfusion CT as a Follow-up Modality After Transcatheter Arterial Chemoembolization. Investigative Radiology, 2010, 45, 427-436.	3.5	55
46	Grading of Cerebral Glioma with Multiparametric MR Imaging and 18F-FDG-PET: Concordance and Accuracy. European Radiology, 2014, 24, 380-389.	2.3	55
47	Correlation of ¹⁸ F-FDG Uptake with Apparent Diffusion Coefficient Ratio Measured on Standard and High b Value Diffusion MRI in Head and Neck Cancer. Journal of Nuclear Medicine, 2011, 52, 1056-1062.	2.8	54
48	Usefulness of MS-MLPA for detection of MGMT promoter methylation in the evaluation of pseudoprogression in glioblastoma patients. Neuro-Oncology, 2011, 13, 195-202.	0.6	51
49	Radiomics prognostication model in glioblastoma using diffusion- and perfusion-weighted MRI. Scientific Reports, 2020, 10, 4250.	1.6	50
50	Transformation of hydrophobic iron oxide nanoparticles to hydrophilic and biocompatible maghemite nanocrystals for use as highly efficient MRI contrast agent. Journal of Materials Chemistry, 2011, 21, 11472.	6.7	49
51	Increased Antiangiogenic Effect by Blocking CCL2-dependent Macrophages in a Rodent Clioblastoma Model: Correlation Study with Dynamic Susceptibility Contrast Perfusion MRI. Scientific Reports, 2019, 9, 11085.	1.6	48
52	Advances in Soft Bioelectronics for Brain Research and Clinical Neuroengineering. Matter, 2020, 3, 1923-1947.	5.0	48
53	Body Fat Assessment Method Using CT Images with Separation Mask Algorithm. Journal of Digital Imaging, 2013, 26, 155-162.	1.6	47
54	CT Differentiation of Cholangiocarcinoma from Periductal Fibrosis in Patients with Hepatolithiasis. American Journal of Roentgenology, 2006, 187, 445-453.	1.0	43

#	Article	IF	CITATIONS
55	The Changes in MGMT Promoter Methylation Status in Initial and Recurrent Glioblastomas. Translational Oncology, 2012, 5, 393-IN19.	1.7	43
56	Bright Vessel Appearance on Arterial Spin Labeling MRI for Localizing Arterial Occlusion in Acute Ischemic Stroke. Stroke, 2015, 46, 564-567.	1.0	43
57	Localized Delivery of Theranostic Nanoparticles and Highâ€Energy Photons using Microneedlesâ€onâ€Bioelectronics. Advanced Materials, 2021, 33, e2100425.	11.1	43
58	Correlation of apparent diffusion coefficient values measured by diffusion MRI and MGMT promoter methylation semiquantitatively analyzed with MSâ€MLPA in patients with glioblastoma multiforme. Journal of Magnetic Resonance Imaging, 2013, 37, 351-358.	1.9	42
59	Central Neurocytoma. Neurosurgery, 2013, 72, 407-414.	0.6	42
60	Cerebral Blood Volume Analysis in Glioblastomas Using Dynamic Susceptibility Contrast-Enhanced Perfusion MRI: A Comparison of Manual and Semiautomatic Segmentation Methods. PLoS ONE, 2013, 8, e69323.	1.1	42
61	Tumor blood flow from arterial spin labeling perfusion MRI: A key parameter in distinguishing highâ€grade gliomas from primary cerebral lymphomas, and in predicting genetic biomarkers in highâ€grade gliomas. Journal of Magnetic Resonance Imaging, 2013, 38, 852-860.	1.9	40
62	Synthetic <scp>MRI</scp> : Technologies and Applications in Neuroradiology. Journal of Magnetic Resonance Imaging, 2022, 55, 1013-1025.	1.9	40
63	Contrast-enhanced MRI T1 Mapping for Quantitative Evaluation of Putative Dynamic Glymphatic Activity in the Human Brain in Sleep-Wake States. Radiology, 2021, 300, 661-668.	3.6	40
64	The Efficacy of Magnetic Resonance Imaging for the Diagnosis of Testicular Rupture: A Prospective Preliminary Study. Journal of Trauma, 2009, 66, 239-242.	2.3	39
65	An NMR metabolomics approach for the diagnosis of leptomeningeal carcinomatosis in lung adenocarcinoma cancer patients. International Journal of Cancer, 2015, 136, 162-171.	2.3	38
66	Lymph Node Metastasis: Ultrasmall Superparamagnetic Iron Oxide–enhanced MR Imaging versus PET/CT in a Rabbit Model. Radiology, 2007, 242, 137-143.	3.6	37
67	Gliomas: Application of Cumulative Histogram Analysis of Normalized Cerebral Blood Volume on 3 T MRI to Tumor Grading. PLoS ONE, 2013, 8, e63462.	1.1	37
68	Imaging of Gastrointestinal Stromal Tumors. Journal of Computer Assisted Tomography, 2004, 28, 596-604.	0.5	35
69	CT Features of an Intraductal Polypoid Mass. Journal of Computer Assisted Tomography, 2006, 30, 173-181.	0.5	35
70	Internal Mammary Arteries Supplying Hepatocellular Carcinoma: Vascular Anatomy at Digital Subtraction Angiography in 97 Patients. Radiology, 2007, 242, 925-932.	3.6	34
71	Hydrotropic magnetic micelles for combined magnetic resonance imaging and cancer therapy. Journal of Controlled Release, 2012, 160, 692-698.	4.8	33
72	T1 Shortening in the Globus Pallidus after Multiple Administrations of Gadobutrol: Assessment with a Multidynamic Multiecho Sequence. Radiology, 2018, 287, 258-266.	3.6	32

#	Article	IF	CITATIONS
73	Imaging and quantification of metastatic melanoma cells in lymph nodes with a ferritin MR reporter in living mice. NMR in Biomedicine, 2012, 25, 737-745.	1.6	31
74	Desmoid-type fibromatosis in the head and neck: CT and MR imaging characteristics. Neuroradiology, 2013, 55, 351-359.	1.1	31
75	Glioma grading using apparent diffusion coefficient map: application of histogram analysis based on automatic segmentation. NMR in Biomedicine, 2014, 27, 1046-1052.	1.6	31
76	Hepatocellular Carcinoma with Internal Mammary Artery Supply: Feasibility and Efficacy of Transarterial Chemoembolization and Factors Affecting Patient Prognosis. Journal of Vascular and Interventional Radiology, 2007, 18, 611-619.	0.2	30
77	Enhancement characteristics of cholangiocarcinomas on mutiphasic helical CT: emphasis on morphologic subtypes. Clinical Imaging, 2008, 32, 114-120.	0.8	30
78	Cervical Lymph Node Metastases: MR Imaging of Gadofluorine M and Monocrystalline Iron Oxide Nanoparticle–47 in a Rabbit Model of Head and Neck Cancer. Radiology, 2006, 241, 753-762.	3.6	29
79	Bandgap engineered reverse type-I CdTe/InP/ZnS core–shell nanocrystals for the near-infrared. Chemical Communications, 2009, , 1267.	2.2	29
80	Clinicopathological and genetic characteristics of extraventricular neurocytomas. Neuropathology, 2013, 33, 111-121.	0.7	29
81	Differentiation of Parkinsonism-Predominant Multiple System Atrophy from Idiopathic Parkinson Disease Using 3T Susceptibility-Weighted MR Imaging, Focusing on Putaminal Change and Lesion Asymmetry. American Journal of Neuroradiology, 2015, 36, 2227-2234.	1.2	29
82	Effect of Delayed Transit Time on Arterial Spin Labeling. Investigative Radiology, 2013, 48, 795-802.	3.5	28
83	Bipolar radiofrequency ablation in ex vivo bovine liver with the open-perfused system versus the cooled-wet system. European Radiology, 2005, 15, 759-764.	2.3	27
84	Prognosis prediction of non-enhancing T2 high signal intensity lesions in glioblastoma patients after standard treatment: application of dynamic contrast-enhanced MR imaging. European Radiology, 2017, 27, 1176-1185.	2.3	27
85	Dynamic contrast-enhanced MR imaging in predicting progression of enhancing lesions persisting after standard treatment in glioblastoma patients: a prospective study. European Radiology, 2017, 27, 3156-3166.	2.3	27
86	Endobronchial metastasis from renal cell carcinoma: CT findings in four patients. European Journal of Radiology, 2004, 51, 155-159.	1.2	26
87	Hepatic Radiofrequency Ablation Using Multiple Probes: Ex Vivo and In Vivo Comparative Studies of Monopolar versus Multipolar Modes. Korean Journal of Radiology, 2006, 7, 106.	1.5	26
88	Radiosurgery for central neurocytoma: long-term outcome and failure pattern. Journal of Neuro-Oncology, 2013, 115, 505-511.	1.4	26
89	Quantitative dynamic contrast-enhanced MR imaging shows widespread blood-brain barrier disruption in mild traumatic brain injury patients with post-concussion syndrome. European Radiology, 2019, 29, 1308-1317.	2.3	26
90	Contrast-Enhanced FLAIR (Fluid-Attenuated Inversion Recovery) for Evaluating Mild Traumatic Brain Injury. PLoS ONE, 2014, 9, e102229.	1.1	25

#	Article	IF	CITATIONS
91	MRI molecular imaging using GLUT1 antibody-Fe3O4 nanoparticles in the hemangioma animal model for differentiating infantile hemangioma from vascular malformation. Nanomedicine: Nanotechnology, Biology, and Medicine, 2015, 11, 127-135.	1.7	25
92	Radiogenomics Profiling for Glioblastoma-related Immune Cells Reveals CD49d Expression Correlation with MRI parameters and Prognosis. Scientific Reports, 2018, 8, 16022.	1.6	25
93	Effect of carotid artery stenting on cerebral blood flow: evaluation of hemodynamic changes using arterial spin labeling. Neuroradiology, 2013, 55, 271-281.	1.1	24
94	Segmentation-Based MR Attenuation Correction Including Bones Also Affects Quantitation in Brain Studies: An Initial Result of ¹⁸ F-FP-CIT PET/MR for Patients with Parkinsonism. Journal of Nuclear Medicine, 2014, 55, 1617-1622.	2.8	24
95	Postbiopsy Splenic Bleeding in a Dog Model: Comparison of Cauterization, Embolization, and Plugging of the Needle Tract. American Journal of Roentgenology, 2005, 185, 878-884.	1.0	23
96	Contrast-Enhanced MR Imaging of Lymph Nodes in Cancer Patients. Korean Journal of Radiology, 2010, 11, 383.	1.5	23
97	Physiological and Functional Magnetic Resonance Imaging Using Balanced Steady-state Free Precession. Korean Journal of Radiology, 2015, 16, 550.	1.5	23
98	Altered Vascular Permeability in Migraine-associated Brain Regions: Evaluation with Dynamic Contrast-enhanced MRI. Radiology, 2019, 292, 713-720.	3.6	23
99	Seizures during the management of high-grade gliomas: clinical relevance to disease progression. Journal of Neuro-Oncology, 2013, 113, 101-109.	1.4	22
100	Application of 3D Fast Spin-Echo T1 Black-Blood Imaging in the Diagnosis and Prognostic Prediction of Patients with Leptomeningeal Carcinomatosis. American Journal of Neuroradiology, 2018, 39, 1453-1459.	1.2	22
101	The value of temozolomide in combination with radiotherapy during standard treatment for newly diagnosed glioblastoma. Journal of Neuro-Oncology, 2013, 112, 277-283.	1.4	21
102	Noninvasive Identification of Viable Cell Populations in Docetaxel-Treated Breast Tumors Using Ferritin-Based Magnetic Resonance Imaging. PLoS ONE, 2013, 8, e52931.	1.1	21
103	Prediction of Prognosis in Glioblastoma Using Radiomics Features of Dynamic Contrast-Enhanced MRI. Korean Journal of Radiology, 2021, 22, 1514.	1.5	21
104	Comparison between the Prebolus T1 Measurement and the Fixed T1 Value in Dynamic Contrast-Enhanced MR Imaging for the Differentiation of True Progression from Pseudoprogression in Glioblastoma Treated with Concurrent Radiation Therapy and Temozolomide Chemotherapy. American Journal of Neuroradiology, 2017, 38, 2243-2250.	1.2	20
105	BCAT1 is a New MR Imaging-related Biomarker for Prognosis Prediction in IDH1-wildtype Glioblastoma Patients. Scientific Reports, 2017, 7, 17740.	1.6	20
106	Differentiation of High-Grade from Low-Grade Astrocytoma: Improvement in Diagnostic Accuracy and Reliability of Pharmacokinetic Parameters from DCE MR Imaging by Using Arterial Input Functions Obtained from DSC MR Imaging. Radiology, 2018, 286, 981-991.	3.6	20
107	MR imaging findings of extraventricular neurocytoma: a series of ten patients confirmed by immunohistochemistry of IDH1 gene mutation. Acta Neurochirurgica, 2012, 154, 1973-1980.	0.9	19
108	<i><scp>IDH2</scp></i> mutation in gliomas including novel mutation. Neuropathology, 2015, 35, 236-244.	0.7	19

#	Article	IF	CITATIONS
109	Early response evaluation for recurrent high grade gliomas treated with bevacizumab: a volumetric analysis using diffusion-weighted imaging. Journal of Neuro-Oncology, 2013, 112, 427-435.	1.4	18
110	Malignant Glioma: MR Imaging by Using 5-Aminolevulinic Acid in an Animal Model. Radiology, 2014, 272, 720-730.	3.6	18
111	Squamous Cell Carcinoma of the Head and Neck: Comparison of Diffusion-weighted MRI at b-values of 1,000 and 2,000 s/mm ² to Predict Response to Induction Chemotherapy. Magnetic Resonance in Medical Sciences, 2015, 14, 337-345.	1.1	18
112	Ultrasonographic Indeterminate Lymph Nodes in Preoperative Thyroid Cancer Patients: Malignancy Risk and Ultrasonographic Findings Predictive of Malignancy. Korean Journal of Radiology, 2020, 21, 598.	1.5	18
113	Diagnostic Accuracy and Confidence of [18F] FDG PET/MRI in comparison with PET or MRI alone in Head and Neck Cancer. Scientific Reports, 2020, 10, 9490.	1.6	17
114	Hyperfunction Thyroid Nodules: Their Risk for Becoming or Being Associated with Thyroid Cancers. Korean Journal of Radiology, 2013, 14, 643.	1.5	16
115	Early Experience of Pre- and Post-Contrast 7.0T MRI in Brain Tumors. Journal of Korean Medical Science, 2013, 28, 1362.	1.1	16
116	Prediction of Response to Concurrent Chemoradiotherapy with Temozolomide in Glioblastoma: Application of Immediate Post-Operative Dynamic Susceptibility Contrast and Diffusion-Weighted MR Imaging. Korean Journal of Radiology, 2015, 16, 1341.	1.5	16
117	Metabolomic comparison between cells overâ€expressing isocitrate dehydrogenase 1 and 2 mutants and the effects of an inhibitor on the metabolism. Journal of Neurochemistry, 2015, 132, 183-193.	2.1	16
118	Loss of Pericytes in Radiation Necrosis after Glioblastoma Treatments. Molecular Neurobiology, 2018, 55, 4918-4926.	1.9	16
119	An NMR Metabolomics Approach for the Diagnosis of Leptomeningeal Carcinomatosis. Cancer Research, 2012, 72, 5179-5187.	0.4	15
120	Prognosis Prediction of Measurable Enhancing Lesion after Completion of Standard Concomitant Chemoradiotherapy and Adjuvant Temozolomide in Glioblastoma Patients: Application of Dynamic Susceptibility Contrast Perfusion and Diffusion-Weighted Imaging. PLoS ONE, 2014, 9, e113587.	1.1	15
121	Recent Application of Advanced MR Imaging to Predict Pseudoprogression in High-grade Glioma Patients. Magnetic Resonance in Medical Sciences, 2016, 15, 165-177.	1.1	15
122	Can Arterial Spin-Labeling with Multiple Postlabeling Delays Predict Cerebrovascular Reserve?. American Journal of Neuroradiology, 2018, 39, 84-90.	1.2	15
123	Improving the Reliability of Pharmacokinetic Parameters at Dynamic Contrast-enhanced MRI in Astrocytomas: A Deep Learning Approach. Radiology, 2020, 297, 178-188.	3.6	15
124	Combined use of susceptibility weighted magnetic resonance imaging sequences and dynamic susceptibility contrast perfusion weighted imaging to improve the accuracy of the differential diagnosis of recurrence and radionecrosis in high-grade glioma patients. Oncotarget, 2017, 8, 20340-20353.	0.8	15
125	Macrophages Homing to Metastatic Lymph Nodes Can Be Monitored with Ultrasensitive Ferromagnetic Iron-Oxide Nanocubes and a 1.5T Clinical MR Scanner. PLoS ONE, 2012, 7, e29575.	1.1	14
126	In Vivo Magnetic Resonance Imaging of Transgenic Mice Expressing Human Ferritin. Molecular Imaging and Biology, 2013, 15, 48-57.	1.3	14

#	Article	IF	CITATIONS
127	Correlation of 11C-methionine PET and diffusion-weighted MRI. Nuclear Medicine Communications, 2014, 35, 720-726.	0.5	14
128	Serial MR Analysis of Early Permanent and Transient Ischemia in Rats: Diffusion Tensor Imaging and High b Value Diffusion Weighted Imaging. Korean Journal of Radiology, 2013, 14, 307.	1.5	13
129	Prognosis of Glioblastoma With Oligodendroglioma Component is Associated With the IDH1 Mutation and MGMT Methylation Status. Translational Oncology, 2014, 7, 712-719.	1.7	13
130	Comparison Between Transauricular and Transfemoral Arterial Access for Hepatic Artery Angiography in a Rabbit Model. Journal of Vascular and Interventional Radiology, 2011, 22, 1181-1187.	0.2	12
131	Inter-Slice Blood Flow and Magnetization Transfer Effects as A New Simultaneous Imaging Strategy. PLoS ONE, 2015, 10, e0140560.	1.1	12
132	Added Value of Computed Tomography to Ultrasonography for Assessing LN Metastasis in Preoperative Patients with Thyroid Cancer: Node-by-Node Correlation. Cancers, 2020, 12, 1190.	1.7	12
133	MGMT Promoter Methylation Status in Initial and Recurrent Glioblastoma: Correlation Study with DWI and DSC PWI Features. American Journal of Neuroradiology, 2021, 42, 853-860.	1.2	12
134	Differentiation between glioblastoma and primary CNS lymphoma: application of DCE-MRI parameters based on arterial input function obtained from DSC-MRI. European Radiology, 2021, 31, 9098-9109.	2.3	12
135	Assessment of Lymph Node Metastases by Contrast-Enhanced MR Imaging in a Head and Neck Cancer Model. Korean Journal of Radiology, 2007, 8, 9.	1.5	11
136	Antiangiogenic Effect of Bevacizumab: Application of Arterial Spin-Labeling Perfusion MR Imaging in a Rat Glioblastoma Model. American Journal of Neuroradiology, 2016, 37, 1650-1656.	1.2	11
137	Assessment of Early Therapeutic Response to Nitroxoline in Temozolomide-Resistant Glioblastoma by Amide Proton Transfer Imaging: A Preliminary Comparative Study with Diffusion-weighted Imaging. Scientific Reports, 2019, 9, 5585.	1.6	11
138	Dynamic Contrast-Enhanced MR Imaging of Nonenhancing T2 High-Signal-Intensity Lesions in Baseline and Posttreatment Glioblastoma: Temporal Change and Prognostic Value. American Journal of Neuroradiology, 2020, 41, 49-56.	1.2	11
139	Assessment of bevacizumab resistance increased by expression of BCAT1 in IDH1 wild-type glioblastoma: application of DSC perfusion MR imaging. Oncotarget, 2016, 7, 69606-69615.	0.8	11
140	Radiological and Clinical Characteristics of a Military Outbreak of Pandemic H1N1 2009 Influenza Virus Infection. Korean Journal of Radiology, 2010, 11, 417.	1.5	10
141	Primary Intracerebral Malignant Fibrous Histiocytoma: CT, MRI, and PET T Findings. Journal of Neuroimaging, 2013, 23, 141-144.	1.0	10
142	Investigation of Inter-Slice Magnetization Transfer Effects as a New Method for MTR Imaging of the Human Brain. PLoS ONE, 2015, 10, e0117101.	1.1	10
143	Application of diffusion-weighted imaging and dynamic susceptibility contrast perfusion-weighted imaging for ganglioglioma in adults: Comparison study with oligodendroglioma. Journal of Neuroradiology, 2016, 43, 331-338.	0.6	10
144	Added Value of Arterial Spin-Labeling MR Imaging for the Differentiation of Cerebellar Hemangioblastoma from Metastasis. American Journal of Neuroradiology, 2017, 38, 2052-2058.	1.2	10

#	Article	IF	CITATIONS
145	Blood-Brain Barrier Disruption in Mild Traumatic Brain Injury Patients with Post-Concussion Syndrome: Evaluation with Region-Based Quantification of Dynamic Contrast-Enhanced MR Imaging Parameters Using Automatic Whole-Brain Segmentation. Korean Journal of Radiology, 2021, 22, 118.	1.5	10
146	Comparison of lymph node metastases assessment With the use of USPIOâ€enhanced MR imaging at 1.5 T versus 3.0 T in a rabbit model. Journal of Magnetic Resonance Imaging, 2010, 31, 134-141.	1.9	9
147	Lymph Node Metastases from Gastric Cancer: Gadofluorine M and Gadopentetate Dimeglumine MR Imaging in a Rabbit Model. Radiology, 2012, 263, 391-400.	3.6	9
148	Paradoxical perfusion metrics of high-grade gliomas with an oligodendroglioma component: quantitative analysis of dynamic susceptibility contrast perfusion MR imaging. Neuroradiology, 2015, 57, 1111-1120.	1.1	9
149	Investigation of control scans in pseudoâ€continuous arterial spin labeling (p <scp>CASL</scp>): Strategies for improving sensitivity and reliability of p <scp>CASL</scp> . Magnetic Resonance in Medicine, 2017, 78, 917-929.	1.9	9
150	Clinical and radiological features of pandemic H1N1 2009 influenza virus infection manifesting as acute febrile respiratory illness at their initial presentations: comparison with contemporaneous non-H1N1 patients. Acta Radiologica, 2011, 52, 410-416.	0.5	8
151	Hypofractionated chemoradiotherapy with temozolomide as a treatment option for glioblastoma patients with poor prognostic features. International Journal of Clinical Oncology, 2015, 20, 21-28.	1.0	8
152	Decreased APE-1 by Nitroxoline Enhances Therapeutic Effect in a Temozolomide-resistant Glioblastoma: Correlation with Diffusion Weighted Imaging. Scientific Reports, 2019, 9, 16613.	1.6	8
153	MRI of magnetically labeled mesenchymal stem cells in hepatic failure model. World Journal of Gastroenterology, 2010, 16, 5611.	1.4	8
154	Prognostic Value of Dynamic Contrast-Enhanced MRI-Derived Pharmacokinetic Variables in Glioblastoma Patients: Analysis of Contrast-Enhancing Lesions and Non-Enhancing T2 High-Signal Intensity Lesions. Korean Journal of Radiology, 2020, 21, 707.	1.5	8
155	Brain Death. Circulation, 2011, 124, 2572-2573.	1.6	7
156	Hollow MnOxPy and Pt/MnOxPy yolk/shell nanoparticles as a T1 MRI contrast agent. Journal of Colloid and Interface Science, 2015, 439, 134-138.	5.0	7
157	Feasibility of Quantifying Arterial Cerebral Blood Volume Using Multiphase Alternate Ascending/Descending Directional Navigation (ALADDIN). PLoS ONE, 2016, 11, e0156687.	1.1	7
158	Leakage correction improves prognosis prediction of dynamic susceptibility contrast perfusion MRI in primary central nervous system lymphoma. Scientific Reports, 2018, 8, 456.	1.6	7
159	Prognostic Prediction Based on Dynamic Contrast-Enhanced MRI and Dynamic Susceptibility Contrast-Enhanced MRI Parameters from Non-Enhancing, T2-High-Signal-Intensity Lesions in Patients with Glioblastoma. Korean Journal of Radiology, 2021, 22, 1369.	1.5	7
160	Computed Tomography Features of an Intraductal Polypoid Mass. Journal of Computer Assisted Tomography, 2006, 30, 18-24.	0.5	6
161	Protective effects of cleavage agents on INS-1 cells against h-IAPP-induced apoptosis. Chemical Communications, 2012, 48, 588-590.	2.2	6
162	Can Amide Proton Transfer MRI Distinguish Benign and Malignant Head and Neck Tumors?. Radiology, 2018, 288, 791-792.	3.6	6

#	Article	IF	CITATIONS
163	Comparison of Genetic Profiles and Prognosis of High-Grade Gliomas Using Quantitative and Qualitative MRI Features: A Focus on G3 Gliomas. Korean Journal of Radiology, 2021, 22, 233.	1.5	6
164	Evaluation of lymph node metastases: Comparison of gadofluorine Mâ€enhanced MRI and diffusionâ€weighted MRI in a rabbit VX2 rectal cancer model. Journal of Magnetic Resonance Imaging, 2012, 35, 1179-1186.	1.9	5
165	Mapping blood flow directionality in the human brain. Magnetic Resonance Imaging, 2016, 34, 754-764.	1.0	5
166	Quad-Contrast Imaging: Simultaneous Acquisition of Four Contrast-Weighted Images (PD-Weighted,) Tj ETQq0 0 Transactions on Medical Imaging, 2021, 40, 3617-3626.	0 rgBT /O 5.4	verlock 10 ⁻ 5
167	Intracranial Metaplastic Meningioma : Clinical and Radiological Characteristics of 11 Cases. Journal of Korean Neurosurgical Society, 2020, 63, 657-663.	0.5	5
168	Augmentation of Chemotherapeutic Infusion Effect by TSU-68, an Oral Targeted Antiangiogenic Agent, in a Rabbit VX2 Liver Tumor Model. CardioVascular and Interventional Radiology, 2012, 35, 168-175.	0.9	4
169	Shoulder sonography after intraarticular fluid injection for evaluation of anterior labral tears: Comparison with conventional sonography. Journal of Clinical Ultrasound, 2013, 41, 94-100.	0.4	4
170	Sclerosing Meningioma : Radiological and Clinical Characteristics of 21 Cases. Journal of Korean Neurosurgical Society, 2016, 59, 584.	0.5	4
171	Brain parenchymal angiomatoid fibrous histiocytoma and spinal myxoid mesenchymal tumor with <i>FET: CREB</i> fusion, a spectrum of the same tumor type. Neuropathology, 2022, 42, 257-268.	0.7	4
172	A Highly Facile and Specific Assay for Cancer-Causing Isocitrate Dehydrogenase Mutant Using ¹³ C ₄ -Labeled α-Ketoglutarate and Heteronuclear NMR. Analytical Chemistry, 2013, 85, 11987-11992.	3.2	3
173	<i>Reply:</i> . American Journal of Neuroradiology, 2018, 39, E126-E126.	1.2	3
174	No Prognostic Impact of Staging Brain MRI in Patients with Stage IA Non–Small Cell Lung Cancer. Radiology, 2022, 303, 632-643.	3.6	3
175	Development of Endovascular Vibrating Polymer Actuator Probe for Mechanical Thrombolysis: A Phantom Study. ASAIO Journal, 2011, 57, 286-292.	0.9	2
176	Development of Endovascular Vibrating Polymer Actuator Probe for Mechanical Thrombolysis. ASAIO Journal, 2012, 58, 503-508.	0.9	2
177	Polymeric Embolization Coil of Bilayered Polyvinyl Alcohol Strand for Therapeutic Vascular Occlusion: A Feasibility Study in Canine Experimental Vascular Models. Journal of Vascular and Interventional Radiology, 2015, 26, 117-123.	0.2	2
178	Evaluation of Tumor Blood Flow Using Alternate Ascending/Descending Directional Navigation in Primary Brain Tumors: A Comparison Study with Dynamic Susceptibility Contrast Magnetic Resonance Imaging. Korean Journal of Radiology, 2019, 20, 275.	1.5	2
179	Cognitive improvement effect of gintonin might be associated with blood-brain barrier permeability enhancement: dynamic contrast-enhanced MRI pilot study. Translational and Clinical Pharmacology, 2021, 29, 21.	0.3	2
180	Myelin Content in Mild Traumatic Brain Injury Patients with Post-Concussion Syndrome: Quantitative Assessment with a Multidynamic Multiecho Sequence. Korean Journal of Radiology, 2022, 23, 226.	1.5	2

#	Article	IF	CITATIONS
181	Benign lymphoepithelial tumor of the pituitary. Neuropathology, 2013, 33, 413-417.	0.7	1
182	A Case Report of Preoperative and Postoperative 7.0T Brain MRI in a Patient with a Small Cell Glioblastoma. Journal of Korean Medical Science, 2014, 29, 1012.	1.1	1
183	Organized Hematoma Developed after Suboccipital Craniectomy. , 2014, 24, 610-612.		1
184	Prognostic Predictions for Patients with Glioblastoma after Standard Treatment: Application of Contrast Leakage Information from DSC-MRI within Nonenhancing FLAIR High-Signal-Intensity Lesions. American Journal of Neuroradiology, 2019, 40, 2052-2058.	1.2	1
185	Multiparametric magnetic resonance imaging features of a canine glioblastoma model. PLoS ONE, 2021, 16, e0254448.	1.1	1
186	Cerebrovascular Reservoir and Arterial Transit Time Changes Assessed by Acetazolamide-Challenged Multi-Phase Arterial Spin Labeling Perfusion MRI in Chronic Cerebrovascular Steno-Occlusive Disease. Journal of the Korean Society of Radiology, 2021, 82, 626.	0.1	1
187	Size control of ferrimagnetic iron oxide nanocubes to achieve optimum static dephasing regime r ₂ relaxivity for in vivo MRI. Proceedings of SPIE, 2012, , .	0.8	0
188	Computational analysis of blood clot dissolution using a vibrating catheter tip. Proceedings of the Institution of Mechanical Engineers, Part H: Journal of Engineering in Medicine, 2012, 226, 337-340.	1.0	0
189	Magnetic resonance enhancement pattern and diagnostic accuracy of gadofluorine M in a rabbit VX2 tumor model: Comparison with gadopentetate dimeglumine. European Journal of Radiology, 2012, 81, 1751-1757.	1.2	0
190	Application of T1 Map Information Based on Synthetic MRI for Dynamic Contrast-Enhanced Imaging: A Comparison Study with the Fixed Baseline T1 Value Method. Korean Journal of Radiology, 2021, 22, 1352.	1.5	0